International Journal of Environmental Science and Technology (2022) 19:6981–6992
https://doi.org/10.1007/s13762-021-03629-z

ORIGINAL PAPER

Copper removal from aqueous solution using raw pine sawdust, olive pomace and their derived traditional biochars

I. Mannaï[1,2] · S. Sayen[1] · A. Arfaoui[3] · A. Touil[2] · E. Guillon[1]

Received: 12 August 2020 / Revised: 21 July 2021 / Accepted: 19 August 2021 / Published online: 4 September 2021
© Islamic Azad University (IAU) 2021

Abstract

In the present study, the ability of four different adsorbents (raw sawdust, raw olive pomace and their derived biochars obtained after pyrolysis) to remove Cu(II) from water was investigated. The derived biochars were prepared using the traditional process of earth mound kilns at a temperature close to 300 °C. The influence of solid charge, contact time, pH, and concentration was studied. The adsorption equilibrium was reached in less than 15 min for sawdust, its biochar, and for olive pomace, and in about 1 h for olive pomace-derived biochar. In the studied conditions where only adsorption occurred in absence of Cu precipitation, the maximum adsorption capacities were determined equal to 4.9, 13.1, 14.9, and 50.8 mg. g^{-1} for olive pomace-biochar, olive pomace, sawdust, and sawdust-biochar, respectively. Thus, the pyrolysis enhanced the adsorption capacities of sawdust but decreased the ones of olive pomace. This study evidenced that raw olive pomace and sawdust as well as their biochar traditionally prepared, may be used as sustainable, low-cost and efficient adsorbents for Cu(II) removal from aqueous solution.

Keywords Adsorbent · Adsorption · Biochar · Cu · Remediation

Introduction

Over the last decades, surface and groundwater pollution has dramatically increased as a result of the release of several pollutants in the environment, such as organic contaminants and metal trace elements (MTE). In particular, the presence of MTE in water is due to the massive use of agro-chemicals in agriculture, mining activities as well as the discharge of wastewater from metallurgic industries in the environment (Blazquez et al. 2005). MTE can also come from natural inputs, such as soil erosion, volcanic eruptions and alteration of bedrock. In addition to water resources contamination, the presence of these pollutants has adverse effects on human health (Fijalkowska et al. 2021, Tomczyk et al. 2020). For instance, ingestion of high quantities of copper in drinking water may cause gastrointestinal bleeding, hypotension, convulsions and significant DNA damages (Yu et al. 2001). Therefore, it is urgent to remove these MTE from water through the use of different technologies, such as precipitation, electrolysis or (bio)sorption (Chakraborty et al. 2020, Cheraghi et al. 2015, Haghighat and Ameri 2016, Tyagi et al. 2020). Among these techniques, (bio)sorption is the least expensive and the most effective technology for removing contaminants from water; the other techniques are likely to generate toxic byproducts and are more difficult to apply on a large scale. Indeed, a wide range of adsorbents, such as activated carbons, zeolites, clays and lignocellulosic materials, have been used for the retention of inorganic pollutants (Miguel et al. 2006, Rajec et al. 2015). Recently, there has been a growing interest for the development of new bio-based, low-cost and sustainable adsorbents (Viglašová et al. 2018) whose production is based on renewable biomass. This is the case of biochar, a carbon-rich solid material obtained through pyrolysis *i.e.* the thermochemical conversion in an oxygen-poor environment (Lehmann and

Editorial responsibility: Anna Grobelak.

✉ S. Sayen
stephanie.sayen@univ-reims.fr

[1] Institut de Chimie Moléculaire de Reims (ICMR), UMR CNRS 7312, Université de Reims Champagne Ardenne, B.P 1039, 51687 Reims Cedex 2, France

[2] Laboratoire de Recherche des Sciences Et Technologies de L'Environnement LRSTE, ISSTE Borj Cédria, B.P 1003, 2050 Hammam Lif, Tunisie

[3] Ecole Supérieure D'Ingénieurs de Medjez El Bab, Unité de Recherche GDRES, Université de Jendouba, Route du Kef Km 5, 9070 Medjez El Bab, Tunisie

Joseph 2009). Indeed, biochar has gained attention since the discovery of the Terra Preta soils (approximately 7000 years old anthropogenic soils) in the Amazon (Parikh et al. 2014). Researchers found out that these soils, initially characterized by a low fertility, had been enriched through historical applications of charcoal, providing them a higher cation exchange capacity and nutrient retention (Sohi et al, 2010). Besides, the contribution of biochar in climate change mitigation through carbon sequestration in soils is the subject of great interest (Agegnehu et al. 2016). For these reasons, much research is focused on the investigation of biochar potential for the remediation of organic and inorganic contaminants in water. Biochars are known as very effective adsorbents (Inyang et al. 2016), and numerous studies considered the valorization of biowastes through biochar production and the use of charred materials for the removal of MTE from water (Yu et al. 2018). A large variety of feedstocks were used for this purpose, such as agricultural wastes (manure, wheat straw, rice husk, waste wood, pistachio, peanut and hazelnut shells), energy crops (corn, wood pellets and oil seed rape), sewage sludge and several other wastes (Sun et al. 2018). Shan et al. (2020) have shown that a biochar obtained from the pyrolysis of peanut shells at 400 °C was very efficient for metal removal from aqueous solution. Indeed, the maximum adsorption capacities of this biochar for Pb^{2+}, Cd^{2+}, Ni^{2+}, Cu^{2+} and Zn^{2+} were between 82 and 239 $mg.g^{-1}$ (Shan et al. 2020). In a similar study, Park et al. (2016) used a biochar produced from sesame straw at 700 °C to eliminate MTE from water. The retained amounts were between 55 and 102 $mg.g^{-1}$ for Pb^{2+}, Cd^{2+}, and Cu^{2+}. Biochars prepared from anaerobically digested sludge (Jin et al. 2016), date seed (Mahdi et al. 2018), rice husk (Masih et al. 2018), orange pomace (Santos et al. 2015), animal manure (Wang et al. 2020), were also used for copper sorption and proved high removal efficiencies. The cationic exchange capacity, the specific surface area, porosity and the pH value of biochars were underlined as the main parameters governing copper adsorption. In the different studies, the physicochemical and structural properties of biochars were shown to be strongly dependent on feedstock nature and pyrolysis conditions, notably temperature, residence time and type of reactors/kilns.

In 2018, 2,894,000 tons of olive oil were produced worldwide (Hogan 2018), and the annual production of wood in the world was estimated to over 3 million cubic metres in 2004 (Planetoscope 2020). Thus, huge amounts of olive pomace (OP) and wood sawdust (SD) are generated every year as the main byproducts of olive oil extraction process and wood industry. A reasonable fraction of these ligno-cellulosic residues can be used as raw materials for biochar preparation. Nevertheless, throughout the scientific literature in this field, biochars were produced in laboratory under controlled pyrolysis conditions. To our knowledge, no study explored the possibility of employing traditionally produced biochars for MTE removal from polluted water, whereas several traditional practices exist since ancient times and are still used today for charcoal production, such as Kon-Tiki kilns in Asia, Brazilian beehive kilns, earth pits and earth mound heaps in Africa (FAO, 2020).

In this context, the aims of the current research work are (i) the traditional production and characterization of biochars prepared from raw OP and pine SD and (ii) the study of their copper adsorption capacities in aqueous solution. The traditional biochars were prepared at Mnihla (Tunisia) in 2018, and copper experiments were carried out at ICMR, UMR CNRS 7312 (Reims, France) in 2019.

Materials and methods

Raw materials

OP and pine SD were collected from an oil mill and a carpentry shop both located in the area of Mnihla (North Tunisia). The collected materials were air-dried, ground and then sieved to 200 µm before undergoing an acido-basic treatment (with 0.1 $mol.L^{-1}$ KOH and 0.1 $mol.L^{-1}$ HNO_3) in order to obtain an insoluble solid in a wide pH range. Finally, both biosolids were washed several times with distilled water and then dried at 40 °C for 48 h.

Biochar preparation

Biochar production in this study was inspired from a traditional method employed by Tunisian farmers to produce charcoal which is locally called "merdouma" (literally means "buried"). In a pottery plate (used to replace the soil stratum needed in the merdouma practice), 250 g of raw materials (OP or SD) was stacked in a small heap, about 25 cm in diameter at the base and 7 cm high. Then, the heap was covered with wood and branches before adding an impermeable layer of wet soil to prevent air entry. A small hole was left at the top of the pile to light the fire to biomass. Once flames appeared, the heap was completely closed to prevent air entry (Fig. 1). Temperature was monitored during the pyrolysis process using an infrared thermometer. The heap was left to cool gradually for half a day, and then opened and biochar was extracted. The obtained biochars (named OP-B and SD-B for OP and pine SD, respectively) were air-dried, ground and then sieved

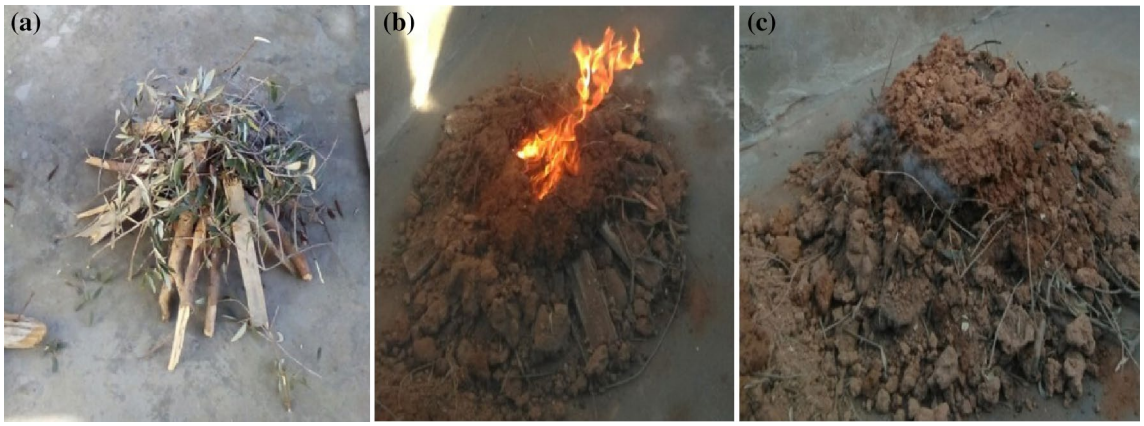

Fig. 1 Photographs of traditional biochar preparation showing heap construction (**a**) firing point (**b**) and white smoke release from the top indicating that fire has taken hold (**c**)

to 200 µm before undergoing an acido-basic treatment in the same way as described for the raw materials.

Characterization of raw materials and biochars

The main physico-chemical properties of raw biosolids and their derived biochars were determined. The pH value was measured for a 1/25 solid/solution ratio in ultra-pure water (ALPHA Q, 18 MΩ cm^{-1}). The specific surface area and the total pore volume were measured using the BET method by N_2 adsorption/desorption at 77 K (Micromeritics ASAP 2020A, United States). Elemental contents of carbon, hydrogen, nitrogen, sulphur (oxygen content was estimated by difference) were determined using an elemental analyzer (CHNS analyzer, Thermo Scientific). The different solids were characterized by Fourier Transform Infrared (FTIR) spectroscopy (Perkin Elmer FTIR Spectrometer) in the transmission mode by dispersing the solids in KBr pellets.

Copper adsorption experiments

The adsorption capacities of the four studied solids (SD, OP, SD-B, OP-B) towards Cu(II) were determined using the batch equilibrium technique at room temperature (293 K) in ultra-pure water (ALPHA Q, 18 MΩ cm^{-1}), and experiments were duplicated. Controls containing Cu(II) without any solid were also prepared to check the absence of retention onto vessels during the whole duration of the experiments. The effects of adsorbent dose (solid charge), contact time, pH and copper initial concentration were investigated.

For experiments as a function of solid charge, 12.5 mg to 100 mg of solid was suspended in 20 mL of ultra-pure water and stirred using an orbital shaker (IKA KS 4000i control) at 200 rpm for 24 h to ensure solid hydration. Then, copper was introduced from a stock solution ($Cu(NO_3)_2$ at 10^{-3} mol.L^{-1} in ultra-pure water) to reach a final concentration of 10^{-4} mol.L^{-1} (6.35 mg Cu.g^{-1}) in a total volume of 25 mL (adjusted by ultra-pure water addition). The suspensions were stirred during 12 h to be sure to reach adsorption equilibrium.

Adsorption kinetic experiments were performed at an introduced Cu concentration of 10^{-4} mol.L^{-1} in a 1 g.L^{-1} suspension (selected after experiments as a function of solid charge) and stirred during a contact time varying in each batch from 15 min to 8 h.

As for experiments as a function of pH, they were carried out at an introduced Cu concentration of 10^{-4} mol.L^{-1} in a 1 g.L^{-1} suspension with varying pH value in each batch from 3 to 9 by dropwise addition of HNO_3 (10^{-1} mol.L^{-1}) or KOH (10^{-1} mol.L^{-1}). The suspensions were stirred for 2 h (equilibrium time deduced from adsorption kinetic experiments).

Finally, experiments as a function of Cu concentration were conducted at 1 g.L^{-1} and pH = 5.3 with an introduced Cu concentration varying between 2. 10^{-5} and 10^{-3} mol.L^{-1} (1.27 to 63.5 mg Cu.L^{-1}) in each batch (2 h stirring).

At the end of each adsorption experiment, the suspensions were filtered through a 0.22 µm cellulose acetate membrane, and the filtrates were acidified with a drop of concentrated nitric acid in order to avoid the metal precipitation in the filtrates before analysis.

The remaining Cu concentration in these filtrates was measured by ICP-OES using an Icap 6300 Duo (Thermo Scientific) in axial mode. Yttrium was used as internal standard and λ = 324.754 and 327.396 nm were selected for Cu. The limits of detection and quantification were equal to 5 and 17 nmol.L^{-1}, respectively. The Cu adsorbed amount was calculated by difference between the introduced and remaining Cu concentrations.

Adsorption isotherm modelling

The Langmuir, Freundlich and Sips adsorption models were used to describe the adsorption isotherms of copper on SD, OP and their derived biochars using Microcal™ Origin® software according to Eqs. 1, 2 and 3, respectively.

$$q_e = q_{\max L}\frac{K_L C_e}{1 + K_L C_e} \quad (1)$$

$$q_e = K_F C_e^n \quad (2)$$

$$q_e = q_{\max S}\frac{K_S C_e^m}{1 + K_S C_e^m} \quad (3)$$

where C_e is the equilibrium copper concentration in solution ($mg.L^{-1}$), q_e is the adsorbed amount of copper per gram of adsorbent at equilibrium ($mg.g^{-1}$), K_L is the Langmuir constant ($L.mg^{-1}$), q_{maxL} is the Langmuir maximum adsorption capacity ($mg.g^{-1}$), K_F ($L^n\ mg^{1-n}\ g^{-1}$) is the Freundlich constant, n is the nonlinearity constant, K_S is the Sips constant ($L^m.mg^{-m}$), q_{maxS} is the Sips maximum adsorption capacity ($mg.g^{-1}$), and m is the Sips model exponent.

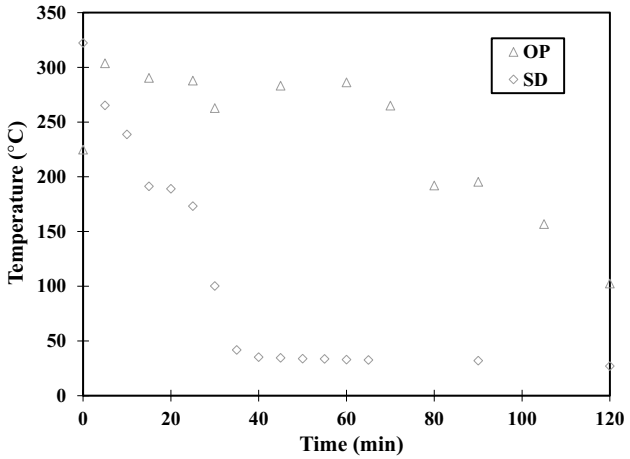

Fig. 2 Temperature evolution during traditional pyrolysis of OP and SD

Results and discussion

Temperature monitoring during traditional pyrolysis

The evolution of temperature in sawdust and olive pomace heaps is reported in Fig. 2. For OP, immediately after ignition, temperature was equal to 224 °C, and within 5 min, it increased to reach a maximum of 303 °C. This phase corresponded to combustion due to air entrapped in the heap which produced heat. Once air was consumed (5 min) the temperature decreased gradually to reach a temperature of 102 °C after cooling. As for SD, the starting temperature was equal to 322 °C, but the cooling phase was much faster than for OP. Indeed, within only half an hour, temperature fell drastically to about 40 °C, to finish at 27 °C after two hours. This rapid cooling suggests that some fresh air was able to get into the sawdust heat during the process. Indeed, during traditional pyrolysis based on earth mound kilns, the earth covering the heap may sink, and any cracks or holes which form must be closed to prevent air leakage (FAO 2020). In our experiment, some small cracks may have formed and would be responsible for the rapid cooling of the sawdust heap.

Characterization of the raw materials and their biochar

Characterization of adsorbents

The composition and main physico-chemical properties of the raw biomasses and their derived biochars are given in Table 1.

The results show that SD and OP presented pH values of 5.8 and 5.3, respectively, comparable to those obtained by other authors, who found a pH of 5.7 for sawdust (Ahmad et al. 2009) and a value of 5.4 for olive pomace (Martinez-Garcia et al. 2006). This acidic nature can be attributed to

Table 1 Composition and physico-chemical properties of the solids

Solid	pH	C (% wt)	N	H	O	S	C/N	O/C	H/C	(O + N)/C	Surface area $m^2.g^{-1}$
SD	5.8	47.4	0.6	6.2	45.6	ns	186.1	0.7	1.5	0.7	1.5
SD-B	9.3	19.3	0.2	1.2	79.1	ns	166.9	3.1	0.8	3.1	4.1
OP	5.3	50.8	1.4	6.8	41.0	ns	83.4	0.6	1.6	0.6	1.4
OP-B	8.1	65.5	1.6	4.7	28.1	ns	92.2	0.3	0.8	0.3	1.6

ns = not significant

the abundance of carboxylic and phenolic moieties at the solid surface. After biomass pyrolysis, their pH values became alkaline (9.3 for SD-B and 8.1 for OP-B). This pH increase after pyrolysis was reported by numerous studies (Nzediegwu et al. 2020) and can be explained by the fact that high temperatures eliminate the acid functional groups present on the surface of biochars (-COOH and -OH) and favour the formation of inorganic carbonates, *e.g.* $MgCO_3$ and $CaCO_3$ (Nanda et al. 2016).

The two raw materials presented similar surface area values (≈ 1.5 $m^2.g^{-1}$). After pyrolysis, the surface area of the sawdust-derived biochar increased to 4.1 $m^2.g^{-1}$, value very close to the one reported by Pariyar et al. (2020) for biochar prepared from sawdust at 350 °C (3.9 $m^2.g^{-1}$). The increase in surface area is generally attributed to the progressive degradation of hemicellulose, cellulose and lignin (Soni and Karmee 2020). In particular, hemicellulose degradation occurs at temperature ranging between 200 and 350 °C (Dorez et al. 2014) and is responsible for a major part of volatile compounds release. Thus, the lower specific surface area of OP-B may be explained by a lower amount of hemicellulose of OP compared to SD (Elalami et al. 2020) leading to a limited thermal degradation.

The elemental analysis showed that the studied raw materials presented relatively similar carbon, nitrogen, hydrogen, and oxygen contents (Table 1). However, after traditional pyrolysis, SD and OP exhibited a different evolution of their elemental composition. Indeed, the C content, which was approximately 50% for both raw materials increased to 65.5% for OP-B, while it dropped down to 19.3% for SD-B. While the increase in C content during pyrolysis is widely accepted among researchers (Chowdhury et al. 2016), the observed strong decrease in the SD-B carbon content was unexpected. Hadroug et al. (2019) also noticed a decrease in the C content in the case of manure-derived biochars, but this loss did not exceed 5–6% and corresponded to a higher process temperature (500–600 °C). These authors attributed this decrease to the presence of labile carbon fraction in the raw materials. In our case for SD-B, the C loss was much higher (around 30%) with a lower temperature (300 °C). It is thus unlikely that this high loss was only due to the removal of labile carbon. Thus, our hypothesis is that, as suggested by temperature profile of SD heap, it is probable that some oxygen entered the artisanal kiln and led to the partial combustion of biomass, hence the decrease in C content of the pyrolyzed SD. According to Lee et al. (2013), the uncontrolled process of biomass burning in open pits (ancient practice), one of the most common processes for biochar production, may produce significant amounts of CO_2 and CO, which can exceed 20% wt. of the C content.

Atomic ratios H/C and O/C or (O + N)/C have been used to investigate the aromaticity (Wang et al. 2015) and polarity (Usman et al., 2015) of biochars. The lower the H/C ratio is, the higher the polycondensation degree of organic compounds. The H/C ratio decreased for both SD-B and OP-B indicating the formation of higher proportions of aromatic C during pyrolysis (Yue et al. 2017), in accordance with previous studies (Stylianou et al. 2020). O/C and (O + N)/C ratios slightly decreased for OP-B suggesting a less polar and hydrophilic character, while they were higher for SD-B indicating an increase in biochar polarity.

Identification of functional groups of raw materials and their biochar by FTIR spectroscopy

SD and OP raw materials spectra (Fig. 3) evidenced an intense broad band centred on 3425 and 3456 cm^{-1}, respectively, attributed to hydroxyl groups corresponding to phenol and alcohol moieties (Ahmed and Khaled, 2019). Their pyrolysis led to the decrease in these bands due to dehydration during the pyrolysis process (Hadroug et al., 2019). Peaks at 2930 and 2925 cm^{-1} for SD and OP, respectively, corresponding to the $\nu_{C\text{-}H}$ stretching band, indicated the presence of hemicellulose and cellulose in raw materials. These peaks disappeared in their biochars, which suggests the degradation of cellulosic compounds during pyrolysis. Broad medium peaks at 1644 and 1634 cm^{-1} for SD and OP, respectively, corresponded to C = O stretching and non-conjugated or aromatic ring C = C stretching vibrations. The intensity of these bands dramatically decreased in their corresponding biochar. The broad medium band around 1385 cm^{-1} in the raw material spectra was attributed to C–H and O–H (phenol) bending vibrations. These bands were strongly modified in the corresponding biochars (decreasing and/or shifted), which may be an indicator of the degradation and depolymerization of cellulose, hemicelluloses and lignin (Cantrell et al. 2012), since these compounds are rich in phenolic groups. Bands between 1300 and 1000 cm^{-1} corresponded mainly to C–O (alcohol, ether, ester … moieties) and C–N (aromatic and aliphatic amines) stretching vibrations.

Copper retention

The adsorption of Cu(II) was studied on raw materials and their corresponding biochars in order to test their performance in the removal of this metallic cation from aqueous solution. In this way, the influence of various parameters was considered.

Effect of solid charge

Four solid/solution ratios from 0.5 to 4 $g.L^{-1}$ were tested for the retention of Cu(II) onto SD, OP, SD-B and OP-B (Fig. 4).

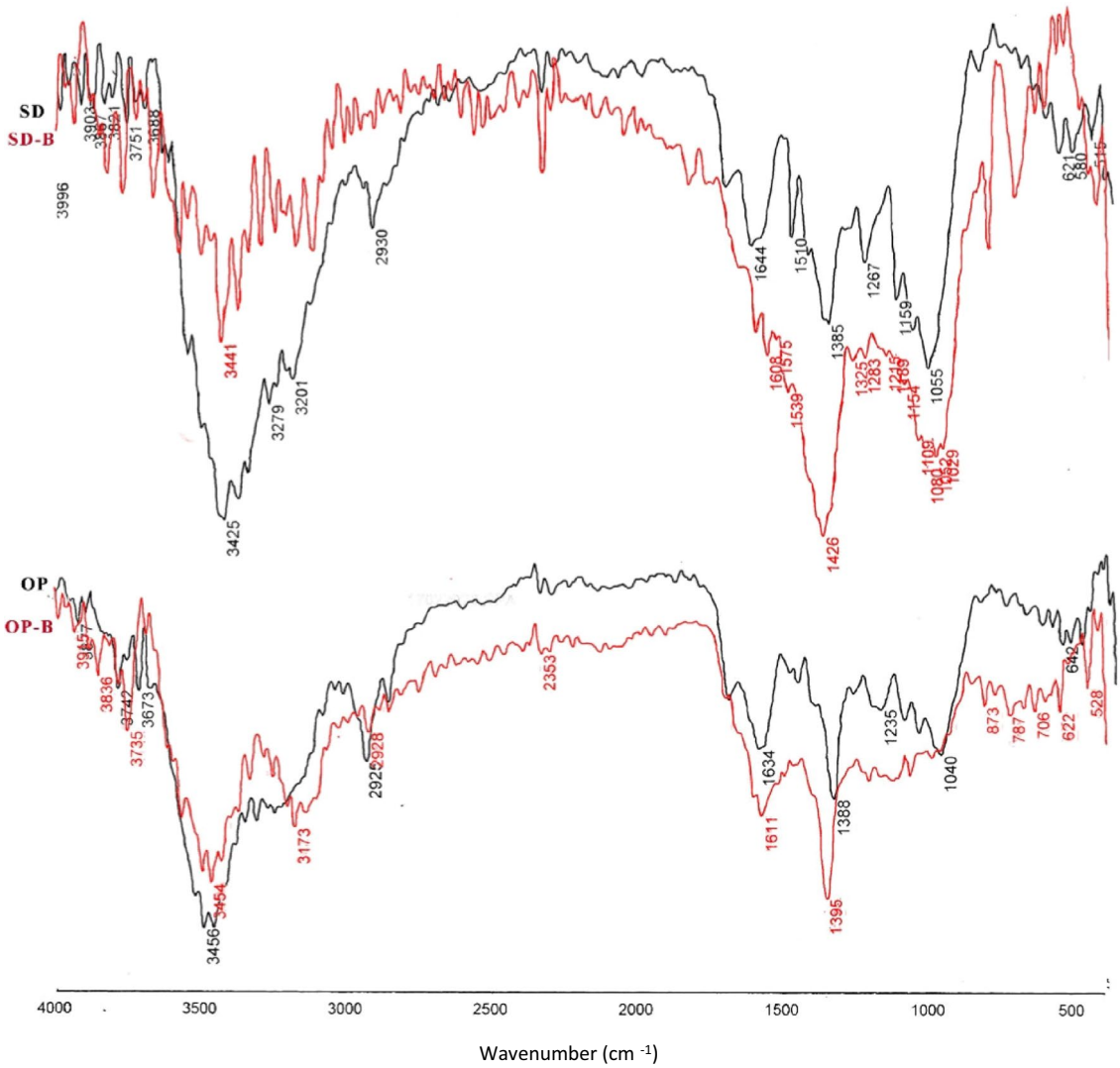

Fig. 3 FTIR spectra of SD, OP and their traditional biochars

As expected, the percentage of adsorbed Cu(II) increased with the solid charge, whereas the adsorbed amount in relation to the total solid weight ($mg.g^{-1}$) decreased. For both solids, the traditional pyrolysis leads to an enhancement of adsorption, in terms of both percentage and amount. A solid charge of 1 $g.L^{-1}$ was selected for further experiments, in order to obtain a good compromise between significant adsorbed amount and percentage.

Effect of contact time

Adsorption kinetic curves obtained at 1 $g.L^{-1}$ for the four solids are reported in Fig. 5.

For all solids, the kinetics were very fast with an adsorption equilibrium time lower than 15 min for SD, SD-B, and OP, and inferior to 1 h for OP-B, corresponding to the beginning of the plateau. For further experiments, the batches were stirred during 2 h in order to have similar conditions for the four solids. As for the percentage of adsorbed Cu(II) at equilibrium, it was greater onto OP (51%) than onto SD (17%). After pyrolysis, these percentages were increased: 1.6 and 5.9 times for OP and SD, respectively. The high enhancement obtained for SD (100% retention onto SD-B) was in accordance with the increased specific surface area (from 1.5 to 4.1 $m^2.g^{-1}$) and pH value (from 5.8 to 9.3) of the solid after pyrolysis.

Effect of pH

The effect of pH on Cu(II) adsorption is presented in Fig. 6 for the four solids.

The adsorption of Cu(II) by raw materials and their biochar classically increased with increasing pH. In the studied conditions, the maximum retention was equal to 75, 95, 100

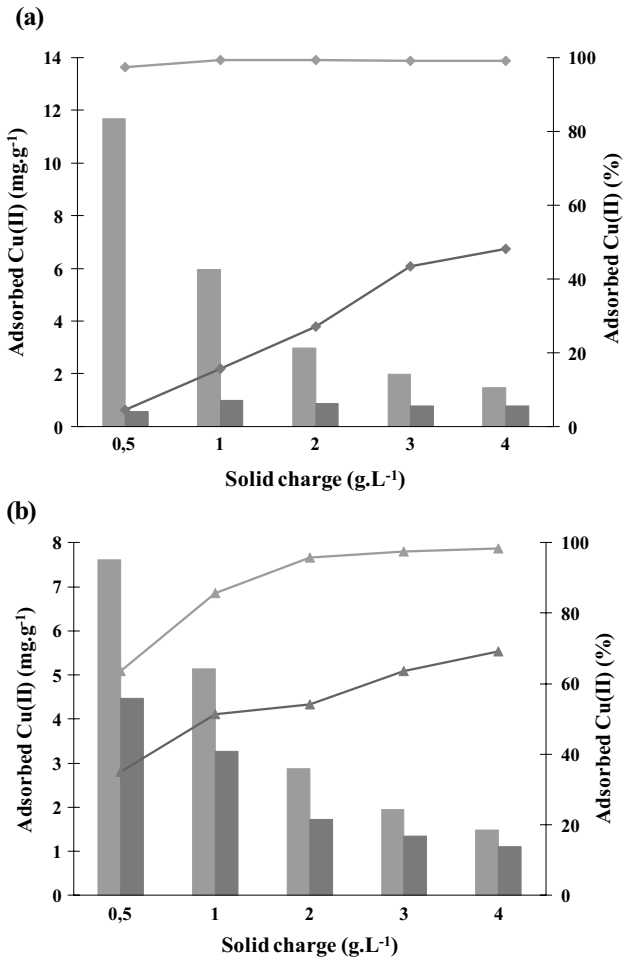

Fig. 4 Effect of solid charge on Cu(II) adsorption onto SD (dark grey), SD-B (light grey) (**a**) and OP (dark grey), OP-B (light grey) (**b**) (histograms in $mg.g^{-1}$ and symbols + lines in %), $[Cu^{2+}]_0 = 10^{-4}$ mol. L^{-1}, contact time = 6 h, T = 20 °C, natural solid pH

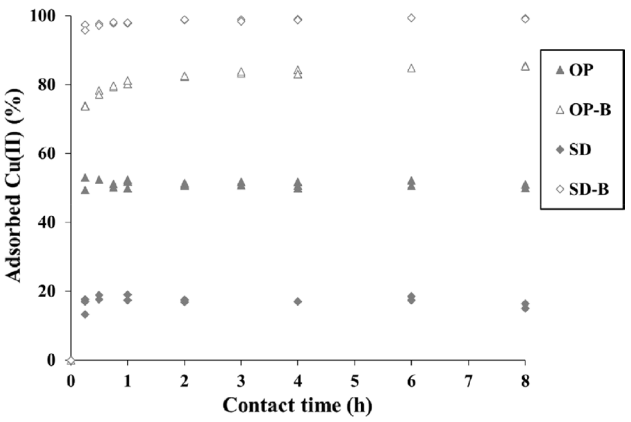

Fig. 5 Adsorption kinetics of Cu(II) onto SB, OP, SD-B, and OP-B ($[Cu^{2+}]_0 = 10^{-4}$ mol.L^{-1}, solid charge = 1 g.L^{-1}, T = 20 °C, natural solid pH)

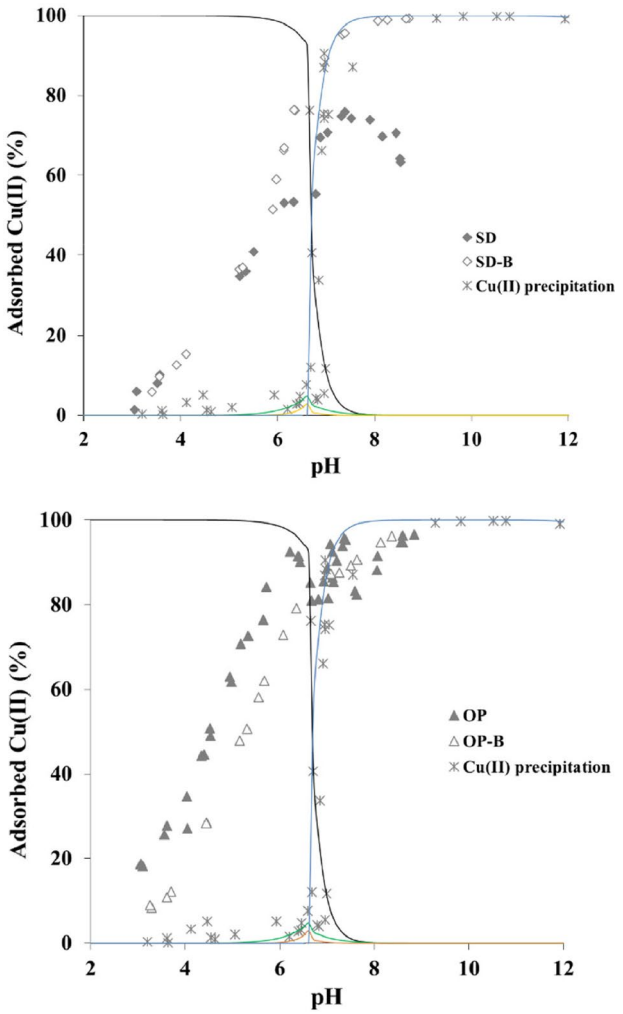

Fig. 6 Effect of pH on Cu(II) retention onto SD, OP, SD-B, and OP-B ($[Cu^{2+}]_0 = 10^{-4}$ mol.L^{-1}, solid charge = 1 g.L^{-1}, T = 20 °C, contact time = 2 h), superimposed with the experimental precipitation curve of Cu(II), and with the speciation diagram of Cu (black = Cu^{2+}, green = $Cu(OH)^{+}$, orange = $Cu_2(OH)_2^{2+}$, blue = $Cu(OH)_{2(s)}$)

and 95% for SD, OP, SD-B, and OP-B, respectively. For comparison, the experimental precipitation curve of Cu(II) is superimposed in Fig. 6. This curve was obtained in the same conditions than adsorption data, but without adding any solid in the batches. This experimental precipitation curve and adsorption data are also superimposed with the speciation diagram of Cu considering the corresponding constants of $Cu(OH)^{+}$ ($\log \beta = -7.9$), $Cu(OH)_2^{0}$ ($\log \beta = -16.8$), $Cu(OH)_3^{-}$ ($\log \beta = -27.5$), $Cu(OH)_4^{2-}$ ($\log \beta = -40.4$), $Cu_2(OH)^{3+}$ ($\log \beta = -5.8$), $Cu_2(OH)_2^{2+}$ ($\log \beta = -11.0$), $Cu_3(OH)_4^{2+}$ ($\log \beta = -22.5$), and $Cu(OH)_{2(s)}$ ($\log K_{sp} = 9.04$) from the constant database IUPAC, and using the HySS program. The experimental precipitation curve was very close to the theoretical curve (blue curve in Fig. 6) and evidenced the precipitation of copper as $Cu(OH)_{2(S)}$ at pH 6.7. Before Cu(II) precipitation, Cu was mainly present as Cu^{2+} cations

(black line in Fig. 6). More than 80% of Cu(II) were retained below the copper precipitation pH value (except for SD at 70%) in accordance with an adsorption process. At higher pH values precipitation cannot be ruled out, and Cu(II) was retained by adsorption and/or precipitation.

In the case of SD, one can notice a decrease in Cu(II) retention above pH 7, certainly due to a partial dissolution of the solid in spite of the preliminary basic treatment. This partial dissolution led to a Cu(II) complexation in solution with released organic compounds instead of copper precipitation, since the percentage of retained copper decreased in basic conditions. This behaviour prevents the use of SD for the removal of Cu(II) in alkaline solutions. The obtained results were in accordance with previous studies reporting that the highest adsorbed amounts onto biochars were generally found between pH 5 and 6 (Bouhamed et al. 2016, Demirbas et al. 2009, Kalavathy et al. 2010).

Cu(II) adsorption capacities

In order to compare the solid removal performances, the influence of the introduced copper concentration on the adsorbed amounts was studied at pH 5.3 in order to obtain adsorption isotherms (Fig. 7). This value far from the Cu(II) precipitation pH value (6.7) was selected (i) to ensure high adsorption capacities according to Fig. 6 and (ii) to prevent the precipitation given that the precipitation pH value is decreased when the initial Cu concentration is increased. The Langmuir and Freundlich classical models were used to fit these isotherms. The adsorption curves relative to OP and OP-B were well fitted with the Langmuir model, whereas the Freundlich model was not suited to describe the data. On the contrary, the adsorbed amounts onto SD and SD-B were well described by the Freundlich model, but not by the Langmuir one (Table 2). In order to compare the performances of the four adsorbents, the adsorption isotherms were thus fitted using the Sips model which is a combined form of Langmuir and Freundlich equations that can simulate both behaviours. It palliates the main drawbacks of these two models: the Langmuir model hypothesizes a homogeneous adsorbent surface with identical adsorption sites, and according to the Freundlich model, infinite adsorbed amounts could be retained on the sorbent surface which is unlikely at solid/liquid interfaces. The Sips model presents the advantage to predict the maximum adsorption capacity of the adsorbent by considering the general case of heterogeneous surfaces (Sips 1948, Sayen et al. 2018). The adsorption data of OP, OP-B, SD and SD-B were very well fitted by this model with determination coefficients R^2 comprised between 0.975 and 0.996 (Fig. 7, Table 2).

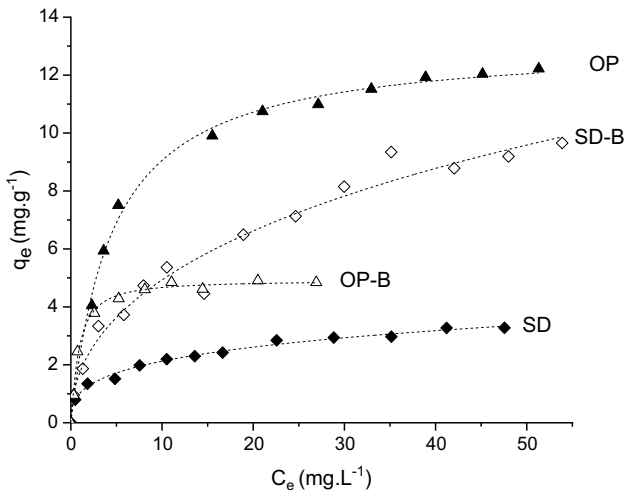

Fig. 7 Equilibrium adsorption isotherms of Cu(II) onto SD, OP, SD-B, and OP-B (symbols), and fitting using Sips model (dotted line), solid charge = 1 g.L^{-1}, T = 20 °C, contact time = 2 h and pH = 5.3

Table 2 Model parameters for the equilibrium isotherms relative to Cu(II) adsorption onto OP, SD and their derived biochars using Langmuir, Freundlich, and Sips models, R^2 = coefficient of determination

Adsorbent	OP	OP–B	SD	SD–B
Langmuir				
q_{maxL} (mg.g^{-1})	13.51	5.00	–	–
K_L (L.mg^{-1})	0.197	1.333	–	–
R^2	0.985	0.995	–	–
Freundlich				
n	–	–	0.31	0.44
K_F (L^n mg^{1-n} g^{-1})	–	–	1.035	1.722
R^2	–	–	0.987	0.978
Sips				
q_{maxS} (mg.g^{-1})	13.12	4.92	14.92	50.82
m	1.00	1.19	0.35	0.48
K_S (L^m.mg^{-m})	0.220	1.216	0.074	0.036
R^2	0.996	0.994	0.993	0.975

The maximum adsorption capacities q_{maxS} predicted by the Sips model increased in the following order: OP-B (4.9 mg.g^{-1}) < OP (13.1 mg.g^{-1}) < SD (14.9 mg.g^{-1}) < SD-B (50.8 mg.g^{-1}) (Table 2). Thus, the pyrolysis of SD enhanced its removal performance (> 3 times), which was not the case for OP, since its pyrolysis led to a reduction in over half from its adsorption capacities. These behaviours could be explained by an increase in both specific surface area (≈ 3 times) and O/C ratio (≈ 4.5 times) after pyrolysis for SD,

Table 3 Comparison of Cu(II) maximum adsorption capacities of various adsorbents from biomass

Material	Experimental conditions	Maximum adsorption capacity ($mg.g^{-1}$)	Reference
SD	pH = 5.3, solid charge = 1 $g.L^{-1}$, T = 20 °C	14.9	This study
OP	pH = 5.3, solid charge = 1 $g.L^{-1}$, T = 20 °C	13.1	This study
SD-B	pH = 5.3, solid charge = 1 $g.L^{-1}$, T = 20 °C	50.8	This study
OP-B	pH = 5.3, solid charge = 1 $g.L^{-1}$, T = 20 °C	4.9	This study
Marine brown alga	pH = 5.5, solid charge = 2 $g.L^{-1}$, T = 22 °C	23.4	(Grimm et al., 2008)
Terrestrial moss	pH = 5.5, solid charge = 2 $g.L^{-1}$, T = 22 °C	11.1	(Grimm et al., 2008)
Birch wood sawdust	pH = 5.5, solid charge = 2 $g.L^{-1}$, T = 22 °C	4.9	(Grimm et al., 2008)
Rice husk	pH = 5.3, solid charge = 5 $g.L^{-1}$, T = 27 °C	29.0	(Wong et al., 2003)
Clay	pH = 6.0, solid charge = 1 $g.L^{-1}$, T = 25 °C	27.6	(Sdiri et al., 2014)
Pine wood pyrolyzed at 300 °C	pH = 6.2, solid charge = 2.5 $g.L^{-1}$, T = 25 °C	4.4	(Liu et al., 2010)

and conversely a diminution of the O/C ratio (2 times) and a similar specific surface area for OP and OP-B.

The maximum adsorption capacities of OP, OP-B, SD, and SD-B, were compared to those of previous studies investigating Cu(II) retention in the most similar experimental conditions and reporting the maximum adsorption capacity of the adsorbent obtained by modelling (*i.e.* in terms of pH value, solid charge, adsorption temperature, and pyrolysis temperature in the case of biochars) but with different biomass-based materials (Table 3). Among the four studied sorbents, SD-B exhibited the highest maximum adsorption capacity which is significantly higher than the sorbents reported in Table 3. This is all the more supported by the fact that the pH value of the other studies was slightly higher than in the present work, which is in favour of an increase in adsorbed amounts.

Concerning the economical aspect, the cost of the traditional biochar can be estimated from the price at which it is sold at the local markets in Tunisia, around 600 USD/ton, while other commercial sorbents, such as activated carbons, are purchased at more than 1200 USD/ton. Thus, the low price of the traditional biochar, very competitive, may increase the interest for this biomaterial and promote its attractiveness as a sorbent for the removal of pollutants from water.

It can thus be concluded that our SD-B artisanal biochar is a competitive biowaste rendering it a good potential candidate as sustainable, low-cost and efficient adsorbent for copper removal from polluted water.

Conclusion

The aim of this work was to investigate the performance of two raw organic wastes (SD and OP) and their derived biochars (SD-B and OP-B) in terms of copper removal from aqueous solution. Biochars were prepared following a soft and easy pyrolysis process traditionally used by Tunisian farmers (earth mound kiln). The physico-chemical characterization of the studied materials showed that the raw biomasses presented initially comparable properties, in terms of pH, elemental composition and specific surface area. After traditional pyrolysis, the charred materials exhibited alkaline pH, higher specific surface areas and more pronounced aromatic character than the source feedstocks. The study of Cu removal by the raw sawdust, olive pomace and their derived biochars showed that regardless of sorbent nature, the uptake of Cu from solution increased with pH and was maximum for alkaline pH values. At pH = 5.3, using a sorbent dose of 1 g/L and a contact time of 2 h, the maximum adsorption capacities deduced from Sips modelling followed the order OP-B ($4.9\ mg.g^{-1}$) < OP ($13.1\ mg.g^{-1}$) < SD ($14.9\ mg.g^{-1}$) < SD-B ($50.8\ mg.g^{-1}$). These behaviours may be explained regarding the specific surface area of the solids and their O/C ratio. The SD-B performance for Cu(II) removal makes it more competitive than biomass-based wastes previously studied in similar conditions.

However, it is worth noticing that the traditional pyrolysis of biomasses still remains an uncontrolled process which may lead to a variability in the quality of the produced biochars and constitutes a barrier to the application of the

traditional pyrolysis at the industrial scale. Thus, as perspectives for this work, the production of biochar from sawdust and olive pomace will be investigated under laboratory controlled conditions in a future study.

Acknowledgements A. Destrebecq is gratefully acknowledged for ICP-OES analyses.

Funding The Ministry of Higher Education and Scientific Research of Tunisia (MERS) is acknowledged for a doctoral research grant awarded to I. Mannai.

Availability of data and material All data will be available under request to the corresponding author.

References

Agegnehu G, Bass AM, Nelson PN, Bird MI (2016) Benefits of biochar, compost and biochar–compost for soil quality, maize yield and greenhouse gas emissions in a tropical agricultural soil. Sci Total Environ 543:295–306. https://doi.org/10.1016/j.scitotenv.2015.11.054

Ahmad A, Rafatullah M, Sulaiman O, Ibrahim MH, Chii YY, Siddique BM (2009) Removal of Cu(II) and Pb(II) ions from aqueous solutions by adsorption on sawdust of Meranti wood. Desalination 247:636–646. https://doi.org/10.1016/j.desal.2009.01.007

Ahmed SK, Khaled S (2019) Syntheses, spectral characterization, thermal properties and DNA cleavage studies of a series of Co(II), Ni(II) and Cu(II) polypyridine complexes with some new imidazole derivatives of 1,10-phenanthroline. Arabian J. Chem. 12:2608–2617. https://doi.org/10.1016/j.arabjc.2015.04.025

Blázquez G, Hernáinz F, Calero M, Ruiz-Núñez LF (2005) Removal of cadmium ions with olive stones: the effect of somes parameters. Process Biochem 40:2649–2654. https://doi.org/10.1016/j.procbio.2004.11.007

Bouhamed F, Elouear Z, Bouzid J, Ouddane B (2016) Multi-component adsorption of copper, nickel and zinc from aqueous solutions onto activated carbon prepared from date stones. Environ Sci Pollut Res 23:15801–15806. https://doi.org/10.1007/s11356-015-4400-3

Cantrell KB, Hunt PG, Uchimiya M, Novak JM, Ro KS (2012) Impact of pyrolysis temperature and manure source on physicochemical characteristics of biochar. Bioresour Technol 107:419–428. https://doi.org/10.1016/j.biortech.2011.11.084

Chakraborty I, Sathe SM, Khuman CN, Ghangrekar MM (2020) Bioelectrochemically powered remediation of xenobiotic compounds and heavy metal toxicity using microbial fuel cell and microbial electrolysis cell. Mater. Sci. Energy Technol. 3:104–115. https://doi.org/10.1016/j.mset.2019.09.011

Cheraghi E, Ameri E, Moheb A (2015) Adsorption of cadmium ions from aqueous solutions using sesame as a low-cost biosorbent: kinetics and equilibrium studies. Int. J. Environ. Sci. Technol 12:2579–2592. https://doi.org/10.1007/s13762-015-0812-3

Chowdhury ZZ, Karim MZ, Ashraf MA, Khalid K (2016) Influence of carbonization temperature on physicochemical properties of biochar derived from slow pyrolysis of durian wood (Durio zibethinus) sawdust. BioResources 11:3356–3372. https://doi.org/10.15376/biores.11.2.3356-3372

Demirbas E, Dizge N, Sulak MT, Kobya M (2009) Adsorption kinetics and equilibrium of copper from aqueous solutions using hazelnut shell activated carbon. Chem Eng J 148:480–487. https://doi.org/10.1016/j.cej.2008.09.027

Dorez G, Ferry L, Sonnier R, Taguet A, Lopez-Cuesta J-M (2014) Effect of cellulose, hemicellulose and lignin contents on pyrolysis and combustion of natural fibers. J. Analyt. Appl. Pyrolysis 107:323–331. https://doi.org/10.1016/j.jaap.2014.03.017

Elalami D, Carere H, Abdelouahdi K, Garcia-Bernet D, Peydecastaing J, Vaca-Medina G, Oukarroum A, Zeroual Y, Barakat A (2020) Mild microwaves, ultrasonic and alkaline pretreatments for improving methane production: impact on biochemical and structural properties of olive pomace. Bioresour Technol 299:122591. https://doi.org/10.1016/j.biortech.2019.122591

FAO (2020). Management of heavy cracking clays FAO SOILS PORTAL Food and Agriculture Organization of the United Nations. IOP publishing FAO SOILS PORTAL http://www.fao.org/soils-portal/soil-management/management-of-some-problem-soils/heavy-cracking-clays/en/. Accessed 10 Agust 2020

Fijałkowska G, Szewczuk-Karpisz K, Wiśniewska M (2021) Polyacrylamide Soil Conditioners: The impact on nanostructured clay minerals' aggregation and heavy metals' circulation in the soil environment. nanomaterials and nanocomposites, nanostructure surfaces, and their applications. https://doi.org/10.1007/978-3-030-51905-6_9

Grimm A, Zanzi R, Björnbom E, Cukierman AL (2008) Comparison of different types of biomasses for copper biosorption. Bioresour Technol 99:2559–2565. https://doi.org/10.1016/j.biortech.2007.04.036

Hadroug S, Jellali S, Leahy JJ, Kwapinska M, Jeuirim M, Hamdi H, Kwapinski W (2019) Pyrolysis process as a sustainable management option of poultry manure: characterization of the derived biochars and assessment of their nutrient release capacities. Water 11:2271. https://doi.org/10.3390/w11112271

Haghighat ZA, Ameri E (2016) Synthesis and characterization of nano magnetic wheat straw for lead adsorption. Desalin. Water Treatm. 57:9813–9823. https://doi.org/10.1080/19443994.2015.1033475

Hogan (2018) Answer to Question No E-006972/17. IOP Publishing European Parliament. https://www.europarl.europa.eu/doceo/document/E-8-2017-006972-ASW_EN.html. Accessed 6 June 2018

MI Inyang, B Gao, Y Yao, Y Yao, Y Xue, A Zimmerman, A Masara, P Pullammanappallil, YS Ok, X Cao. 2016. A review of biochar as a low-cost adsorbent for aqueous heavy metal removal. Crit Rev Environm Sci Technol. 46 406 433 https://doi.org/10.1080/10643389.2015.1096880

Jin H, Hanif MU, Capareda S, Chang Z, Huang H, Ai Y (2016) Copper(II) removal potential from aqueous solution by pyrolysis biochar derived from anaerobically digested algae-dairy-manure and effect of KOH activation. J Environ Chem Eng 4:365–372. https://doi.org/10.1016/j.jece.2015.11.022

Kalavathy MH, Miranda LR (2010) Comparison of copper adsorption from aqueous solution using modified and unmodified hevea brasiliensis saw dust. Desalination 255:165–174. https://doi.org/10.1016/j.desal.2009.12.028

Lee JW, Hawkins B, Li X, Day DM (2013) Biochar Fertilizer for Soil Amendment and Carbon Sequestration. In: Lee JW (ed) Advanced Biofuels and Bioproducts, edn. Springer, New York, pp 57–68

Lehmann L, Joseph S (2009) Biochar for environmental management: An introduction. In: Lehmann L, Joseph S (eds) Biochar for

Environmental Management: Science, Technology and Implementation, 2cd edn. Routledge, London, pp 1–12
Liu Z, Zhang FS, Wu J (2010) Characterization and application of chars produced from pinewood pyrolysis and hydrothermal treatment. Fuel 89:510–514. https://doi.org/10.1016/j.fuel.2009.08.042
Mahdi Z, Yu QJ, El Hanandeh A (2018) Investigation of the kinetics and mechanisms of nickel and copper ions adsorption from aqueous solutions by date seed derived biochar. J Environ Chem Eng 6:1171–1181. https://doi.org/10.1016/j.jece.2018.01.021
Martinez-Garcia G, Bachmann RTh, Williams CJ, Burgoyne A, Edyvean RGJ (2006) Olive oil waste as a biosorbent for heavy metals. Int Biodeterior Biodegrad 58:231–238. https://doi.org/10.1016/j.ibiod.2006.06.028
Masih M, Anthony P, Siddiqui SH (2018) Removal of Cu (II) ion from aqueous solutions by Rice Husk Carbon-Chitosan Composite gel (CCRH) using response surface methodology. Environ. Nanotechnol. Monitor. Manag. 10:189–198. https://doi.org/10.1016/j.enmm.2018.07.003
Miguel GS, Lambert SD, Graham NJ (2006) A practical review of the performance of organic and inorganic adsorbents for the treatment of contaminated waters. J Chem Technol Biotechnol 81:1685–1696. https://doi.org/10.1002/jctb.1600
Nanda S, Dalai AK, Berruti F, Kozinski JA (2016) Biochar as an Exceptional Bioresource for Energy, Agronomy, Carbon Sequestration, Activated Carbon and Specialty Materials. Waste Biomass Valor. 7:201–235. https://doi.org/10.1007/s12649-015-9459-z
Nzediegwu C, Arshad M, Ulah A, Naeth MA, Chang SX (2020) Fuel, thermal and surface properties of microwave-pyrolyzed biochars depend on feedstock type and pyrolysis temperature. Bioresou Technol. https://doi.org/10.1016/j.biortech.2020.124282
Parikh SJ, Goyne KW, Margenot AJ, Mukome FND, Calderón FJ (2014) Chapter One - Soil Chemical Insights Provided through Vibrational Spectroscopy. Adv Agron 126:1–148. https://doi.org/10.1016/B978-0-12-800132-5.00001-8
Pariyar P, Kumari K, Jain MK, Jadhao PS (2020) Evaluation of change in biochar properties derived from different feedstock and pyrolysis temperature for environmental and agricultural application. Sci Total Environ 713:136433. https://doi.org/10.1016/j.scitotenv.2019.136433
Park JH, Ok YS, Kim S-H, Cho J-S, Heo J-S, Delaunee RD, Seo D-C (2016) Competitive adsorption of heavy metals onto sesame straw biochar in aqueous solutions. Chemosphere. https://doi.org/10.1016/j.chemosphere.2015.05.093
Planetoscope (2020) Statistiques : Production de bois dans le monde. IOP Publishing Conso Planetoscope Globe. https://www.planetoscope.com/forets/279-production-de-bois-dans-le-monde.html. Accessed 10 August 2020.
Rajec P, Galamboš M, Daňo M, Rosskopfová O, Čaplovičová M, Hudec P, Horňáček M, Novák I, Berek D, Čaplovič Ľ (2015) Preparation and characterization of adsorbent based on carbon for pertechnetate adsorption. J Radioanal Nucl Chem 303:277–286. https://doi.org/10.1007/s10967-014-3303-y
Santos CM, Dweck J, Viotto RS, Rosa AH, Morais LC (2015) Application of orange peel waste in the production of solid biofuels and biosorbents. Bioresour. Technol. 196:469–479. https://doi.org/10.1016/j.biortech.2015.07.114
Sayen S, Ortenbach-Lopez M, Guillon E (2018) Sorptive removal of enrofloxacin antibiotic from aqueous solution using a lignocellulosic substrate from wheat bran. J Environ Chem Eng 6:5820–5829
Sdiri AT, Higashi T, Jamoussi F (2014) Adsorption of copper and zinc onto natural clay in single and binary systems. Int. J. Environ. Sci. Technol 11:1081–1092. https://doi.org/10.1007/s13762-013-0305-1
Shan R, Shi Y, Gu J, Wang Y, Yuan H (2020) Single and competitive adsorption affinity of heavy metals toward peanut shell-derived biochar and its mechanisms in aqueous systems. Chin J Chem Eng 28:1375–1383. https://doi.org/10.1016/j.cjche.2020.02.012
Sips R (1948) Combined form of Langmuir and Freundlich equations. J Chem Phys 16:490–495
Sohi SP, Krull E, Lopez-Capel E, Bol R (2010) A review of biochar and its use and function in soil. Adv Agron 105:47–82. https://doi.org/10.1016/S0065-2113(10)05002-9
Soni B, Karmee SK (2020) Towards a continuous pilot scale pyrolysis based biorefinery for production of biooil and biochar from sawdust. Fuel 271:117570. https://doi.org/10.1016/j.fuel.2020.117570
Stylianou M, Christou A, Dalias P, Polycarpou P, Michael C, Agapiou A, Papanastasiou P, Fatta-Kassinos D (2020) Physicochemical and structural characterization of biochar derived from the pyrolysis of biosolids, cattle manure and spent coffee grounds. J Energy Inst. https://doi.org/10.1016/j.joei.2020.05.002
Sun P, Li Y, Meng T, Zhang R, Song M, Ren J (2018) Removal of sulfonamide antibiotics and human metabolite by biochar and biochar/H_2O_2 in synthetic urine. Water Res 147:91–100. https://doi.org/10.1016/j.watres.2018.09.051
Tomczyk A, Szewczuk-Karpisz K, Sokołowska Z, Kercheva M, Dimitrov E (2020) Purification of aqueous media by biochars: feedstock type effect on silver nanoparticles removal. Molecules 25:2930. https://doi.org/10.3390/molecules25122930
Tyagi S, Malik W, Annachhatre AP (2020) Heavy metal precipitation from sulfide produced from anaerobic sulfidogenic reactor. Mater Today: Proceed. https://doi.org/10.1016/j.matpr.2020.05.076
Usman ARA, Abduljabbar A, Vithanaage M, OK YS, Ahmad M, Ahmad M, Elfaki J, Abdulazeem SS, Al-Wabel MI (2015) Biochar production from date palm waste: Charring temperature induced changes in composition and surface chemistry. J Anal Appl Pyrolysis 115:392–400. https://doi.org/10.1016/j.jaap.2015.08.016
Viglašová E, Galamboš M, Danková Z, Krivosudský L, Lengauer CL, Hood-Nowotny R, Soja G, Rompel A, Matík M, Briančin J (2018) Production, characterization and adsorption studies of bamboo-based biochar/montmorillonite composite for nitrate removal. Waste Manag. 79:385–394. https://doi.org/10.1016/j.wasman.2018.08.005
Wang X, Zhou W, Liang G, Song D, Zhang X (2015) Characteristics of maize biochar with different pyrolysis temperatures and its effects on organic carbon, nitrogen and enzymatic activities after addition to fluvo-aquic soil. Sci Total Environ 538:137–144. https://doi.org/10.1016/j.scitotenv.2015.08.026
Wang S, Kwak JH, Islam MS, Naeth MA, Gamal El-Din M, Chang SX (2020) Biochar surface complexation and Ni(II), Cu(II), and Cd(II) adsorption in aqueous solutions depend on feedstock type. Sci Total Environ 712:136538. https://doi.org/10.1016/j.scitotenv.2020.136538

Wong KK, Lee CK, Low KS, Haron MJ (2003) Removal of Cu and Pb by tartaric acid modified rice husk from aqueous solutions. Chemosphere 50:23–28. https://doi.org/10.1016/S0045-6535(02)00598-2

Yu B, Zhang Y, Shukla A, Shukla SS, Dorris KL (2001) The removal of heavy metals from aqueous solutions by sawdust adsorption — removal of lead and comparison of its adsorption with copper. J Hazard Mater 84:83–94. https://doi.org/10.1016/S0304-3894(01)00198-4

Yu W, Lian F, Cui G, Liu Z (2018) N-doping effectively enhances the adsorption capacity of biochar for heavy metal ions from aqueous solution. Chemosphere 193:8–16. https://doi.org/10.1016/j.chemosphere.2017.10.134

Yue Y, Lin Q, Xu Y, Li G, Zhao X (2017) Slow pyrolysis as a measure for rapidly treating cow manure and the biochar characteristics. J Anal Appl Pyrolysis 124:355–361. https://doi.org/10.1016/j.jaap.2017.01.008